

Going beyond explainability in multi-modal stroke outcome prediction models

Jonas Brändli^{1,*}, Maurice Schneeberger^{2,*}, Lisa Herzog^{3,4}, Loran Avci¹, Nordin Dari¹, Martin Hänsel^{2,3}, Hakim Baazaoui³, Pascal Bühler¹, Susanne Wegener^{3,4}, Beate Sick^{1,2}

¹ Zurich University of Applied Sciences, Institute of Data Analysis and Process Design (IDP),
Technikumstrasse 9, 8401 Winterthur, Switzerland

² University of Zurich, Epidemiology, Biostatistics and Prevention Institute (EBPI), Hirschengraben
84, 8001 Zurich, Switzerland

³ University Hospital Zurich, Department of Neurology, Frauenklinikstrasse 26, 8091 Zurich,
Switzerland

⁴ University of Zurich, Faculty of Medicine, Pestalozzistrasse 3, 8032 Zurich, Switzerland

Key points:

- Multi-modal outcome prediction models with explainable image and interpretable tabular part
- Identification of relevant image regions for outcome prediction and error analyses.

Key words:

Trustworthy prediction models, Explanation maps, multi-modal neural network models, deep transformation models, similarity plots, stroke

* contributed equally

° corresponding author: lisa.herzog@uzh.ch

Abstract

Aim: This study aims to enhance interpretability and explainability of multi-modal prediction models integrating imaging and tabular patient data.

Methods: We adapt the xAI methods Grad-CAM and Occlusion to multi-modal, partly interpretable deep transformation models (dTMs). DTMs combine statistical and deep learning approaches to simultaneously achieve state-of-the-art prediction performance and interpretable parameter estimates, such as odds ratios for tabular features. Based on brain imaging and tabular data from 407 stroke patients, we trained dTMs to predict functional outcome three months after stroke. We evaluated the models using different discriminatory metrics. The adapted xAI methods were used to generate explanation maps for identification of relevant image features and error analysis.

Results: The dTMs achieve state-of-the-art prediction performance, with area under the curve (AUC) values close to 0.8. The most important tabular predictors of functional outcome are functional independence before stroke and NIHSS on admission, a neurological score indicating stroke severity. Explanation maps calculated from brain imaging dTMs for functional outcome highlighted critical brain regions such as the frontal lobe, which is known to be linked to age which in turn increases the risk for unfavorable outcomes. Similarity plots of the explanation maps revealed distinct patterns which give insight into stroke pathophysiology, support developing novel predictors of stroke outcome and enable to identify false predictions.

Conclusion: By adapting methods for explanation maps to dTMs, we enhanced the explainability of multi-modal and partly interpretable prediction models. The resulting explanation maps facilitate error analysis and support hypothesis generation regarding the significance of specific image regions in outcome prediction.

1 Introduction

Models for outcome prediction in medical applications are supposed to be trustworthy, i.e., they have to (i) capture the health status of a patient adequately, for example by considering imaging and tabular data, (ii) yield a high prediction performance, and (iii) be interpretable [1]. Classical statistical models are trustworthy in terms of providing interpretable parameter estimates along with measures of uncertainty for the single input features. Yet, these models are restricted to tabular data and often sacrifice prediction performance in favor of transparency. In contrast, deep learning (DL) models show an outstanding prediction performance on imaging data but have a black-box character.

Recently developed deep Transformation Models (dTMs) unite statistical with deep learning approaches [2, 3] while modeling each input modality with a (potentially deep) neural network (NN, s. Figure 2). They provide interpretable parameter estimates for tabular features and achieve state-of-the-art prediction performance with deep NNs for imaging data [4], even outperforming expert neurologists [5]. Although dTMs show a considerably higher degree of interpretability compared to other neural network based, multi-modal models [6], the part relying on imaging data remains a black-box. Explainable artificial intelligence (xAI) approaches were developed to better understand DL-based predictions. These models determine the importance of inputs after predictions were made. This can result in a lack of robustness and reliability [1, 7]. Nonetheless, as long as DL models for image data significantly outperform interpretable models that use extracted image features, DL models cannot be abandoned, and using xAI methods is the only possibility to shed some light into the black box.

In this work, we extend the xAI methods Occlusion [8] and Grad-CAM [9] to dTMs to highlight image regions relevant for outcome prediction (s. Figure 1). We demonstrate the applicability when predicting functional outcome using brain imaging and tabular data of patients with an ischemic event. We assess the models in terms of prediction performance, explainability and interpretability. We show how different classes of explanation patterns can be identified, which may serve as the basis for generating novel hypotheses about the importance of specific brain regions.

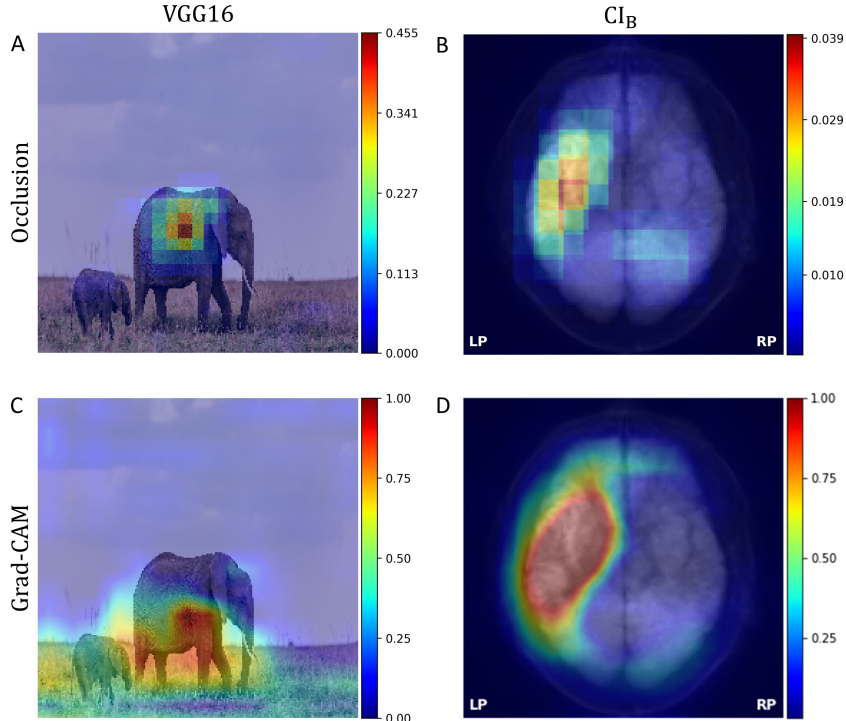


Figure 1: Examples of images overlaid with explanation maps resulting from the xAI methods Occlusion (upper row) and Grad-CAM (lower row). The images on the left are classified as "African elephant" with a VGG16 architecture trained on Imagenet [10]. The images on the right represent an average image over a brain volume of a stroke patient predicted having an "unfavorable" outcome using a dTM (CI_B model) trained on diffusion weighted images. The colors in the legend highlight the importance of the image region for the respective prediction (larger values indicate higher relevance).

2 Materials and methods

2.1 Data

We retrospectively collected data of 407 patients administered to the University Hospital of Zurich between 2014 and 2018 due to an ischemic event. The cohort consists of $n=295$ ischemic stroke and $n=112$ transient ischemic attack patients. Functional outcome at three months after stroke is assessed using the modified Rankin Scale (mRS) score, categorized into favorable (mRS 0-2, $n=332$ patients) vs. unfavorable (mRS 3-6, $n=75$ patients) outcome. Diffusion Weighted Imaging (DWI) was performed in all patients within three days after symptom onset. For analysis, the brain volumes were preprocessed to have dimension $128 \times 128 \times 28$, zero mean and unit standard deviation. Tabular predictors known to be associated with functional outcome and included into the models are age and sex, risk factors, such as coronary heart disease (CHD), hypertension, diabetes, atrial fibrillation, prior stroke or TIA, smoking and hypercholesterolemia as well as on admission information like the national institute of health stroke scale (NIHSS) and pre stroke mRS indicating stroke severity and functional independence prior to the event. To ensure comparability of derived parameter estimates, categorical variables were dummy-encoded and numerical variables standardized. Ethical approval for this study was obtained from the cantonal Ethics Committee.

2.2 Models

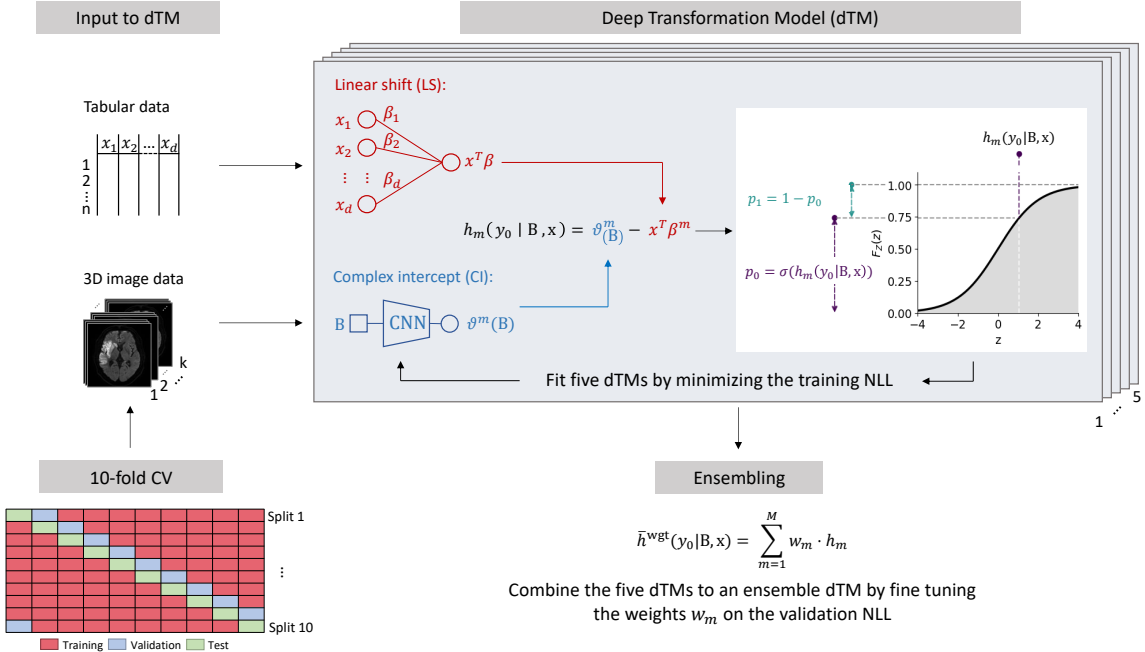


Figure 2: Deep transformation model training and evaluation setup. We perform a 10-fold cross-validation by repeating the following steps for each split. We provide tabular and imaging data as input to the NNs of the dTM. The NNs are trained jointly by minimizing the NLL to learn the parameters of the transformation function h_m . For binary outcomes, h_m represents a cutpoint to separate the standard logistic distribution with $F_Z(z) = \sigma(z)$, yielding a probability for favorable $p_0 = \sigma(h_m(y_0 | B, x))$ vs. unfavorable ($1 - p_0$) outcome (right panel). Models with imaging data are fitted $m = 5$ times on the training data of the respective split, each time with a new random initialization of NN weights. These five models are averaged to an ensemble dTM by calculating a weighted average across the five transformation functions \bar{h}^{wgt} .

Architecture of a multi-modal dTM with binary outcome: To bridge the gap between interpretable statistical models for tabular data with limited prediction performance and accurate black-box deep learning models for image data, we developed deep Transformation Models (dTM) for multi-modal inputs (s. Figure 2) [2]. DTMs are probabilistic models which learn a conditional probability

distribution $F_{Y|\text{input}}$ for an outcome Y . Instead of estimating the outcome distribution directly, they estimate a transformation function h , transforming a predefined latent distribution F_Z into $F_{Y|\text{input}}$ such that $F_{Y|\text{input}}(y) = F_Z(h(y|\text{input}))$. F_Z is a parameter-free probability distribution defining the interpretational scale of the parameters in h [11, 2]. In this work, we choose a standard logistic distribution with $F_Z(z) = \sigma(z)$ being the sigmoid which enables us to interpret the parameters of h as log-odds ratios like in standard logistic regression [11]. The transformation model framework is particularly useful because we can model different outcome distributions and change the interpretability of resulting parameter estimates by using different latent distributions F_Z .

In our binary outcome setting, h represents a cutpoint $h(y_0|\text{input})$ for $F_Z = \sigma$ which determines the probabilities for a favorable y_0 and unfavorable outcome y_1 (s. Figure 2) with

$$p_0 = P(y_0|\text{input}) = \sigma(h(y_0|\text{input})) \quad \text{and} \quad p_1 = 1 - \sigma(h(y_0|\text{input})).$$

We can trade off interpretability and complexity of dTMs by using simple (SI) or complex intercept (CI) terms and adding linear (LS) or complex shift (CS) terms to the models [2]. The intercept terms determine the shape of the transformation function (location of the cutpoint in the case of a binary outcome) while the shift terms enable to shift the function up and downwards depending on the input.

Implemented versions of dTMs with binary outcome: To model our brain images \mathbf{B} and tabular data x , we consider the following models:

- A simple intercept (**SI**) dTM with $h(y_0) = \vartheta_0$, which is equal to a null model without input data estimating the proportion of favorable outcomes to evaluate if the input data is useful for outcome prediction.
- A **SI-LS_x** dTM with $h(y_0|x) = \vartheta_0 + x^T\beta$ which comprises a simple intercept and linear shift term based on tabular data. This model is equal to a standard logistic regression. Here, we allow the transformation function to be shifted by the tabular data and therefore the outcome distribution to vary for different tabular inputs.
- A **CI_B** dTM with $h_m(y_0|\mathbf{B}) = \vartheta_0(\mathbf{B})$ featuring a complex intercept (CI) that is modeled with a 3D CNN.
- A **CI_B-LS_x** dTM with $h(y_0|\mathbf{B}, x) = \vartheta_0(\mathbf{B}) + x^T\beta$ in which the transformation function/cut point is estimated with a 3D CNN and can further be shifted up or downwards based on tabular data.

The NN architectures used to estimate the terms in h are summarized in the supplemental material. All NNs in the dTM are jointly trained by minimizing the negative log likelihood (NLL) for binary outcomes.

Interpretable deep ensembling: To enhance prediction performance without losing interpretability, we perform deep ensembling [12] for those dTMs relying on imaging data. Therefore, we train a dTM m times on the training data using a different random initialization of neural network weights each time. This yields m different transformation functions h_m . Then, we determine a joint transformation function for the ensemble dTM which is a weighted average of the m transformation functions such that

$$\bar{h}^{wgt} = \sum_{m=1}^M w_m h_m.$$

The weights w_m are tuned to minimize the NLL on the validation data.

In case of a fully interpretable SI-LS_x dTM with $h(y_0|x) = \vartheta_0 + x^T\beta$, the interpretable ensemble relies on $\bar{h}^{wgt} = \sum_{m=1}^M w_m \vartheta_0 + x^T(\sum_{m=1}^M w_m \beta_m) = \bar{\vartheta}_0^{wgt} + x^T \bar{\beta}^{wgt}$ which again yields interpretable parameters $\bar{\beta}_k^{wgt}$ quantifying the effect of the k -th predictor x_k on the outcome.

2.3 Evaluation

All models are evaluated in a stratified 10-fold cross validation (CV) (s. Figure 2). Test performances are assessed using the NLL and AUC as well as specificity, sensitivity, accuracy and F1-score. For the specificity, sensitivity and accuracy 95% Wilson confidence intervals are determined. For the NLL,

AUC and F1 score bootstrap CIs were computed. The thresholds to transform the predicted probability into the predicted class are chosen such that the geometric mean of true positive and negative rates are maximized on the validation data of the respective CV split. All code to reproduce the findings is available under https://github.com/liherz/xAI_paper.

2.4 Explanation maps

For visual explanation, we have adapted the xAI methods Grad-CAM [9] and Occlusion [8] to dTMs (s. Figure 3 for an overview).

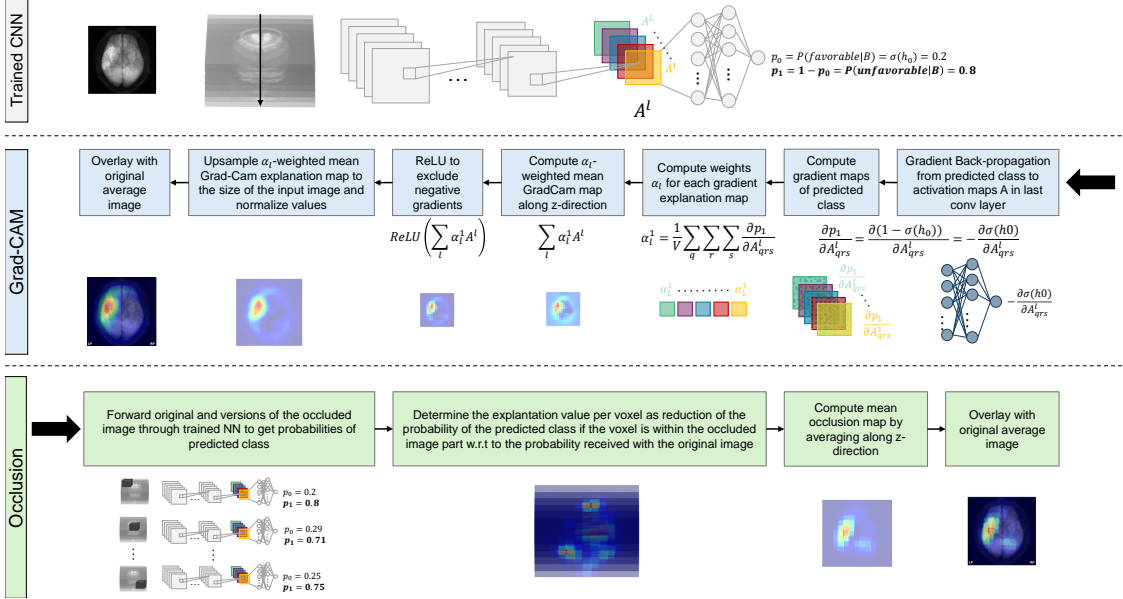


Figure 3: Overview of the Grad-CAM and Occlusion method adapted to dTMs. The trained CNN builds the basis for both methods. Grad-CAM uses the gradient information flowing back from the predicted class to the last convolutional layer to determine input feature importance. Occlusion systematically covers parts of the input to then highlight the changes in predicted probability for a respective class.

Grad-CAM: In its original form, Grad-CAM makes use of gradient information flowing from the output node for the predicted class k into the last convolutional layer of a 2D CNN. The activation maps A of this layer are assumed to represent high-level semantic features and information about feature location in the input. First, importance of each 2D activation map A^l in this layer is determined by quantifying and pooling the gradient based pixel importance $\frac{\partial p_k}{\partial A_{(r,s)}^l}$ for outcome prediction. This gives one importance measure per map which is used as weight when averaging all activation maps to a first version of the explanation map. Then, all negative entries are removed to highlight regions supporting the predicted class only. Upsampling to the original input size yields the desired explanation map for the predicted class.

In our dTMs the output node of the 3D CNN does not yield a class probability but a component of the transformation function h (s. Figure 2) requiring an adjustment of the algorithm (s. Figure 3). To quantify importance of a 3D activation map A^l , $l = 1, \dots, L$ in the last convolutional layer of a 3D CNN, we first calculate importance of each voxel $A_{(q,r,s)}^l$, here shown for a $\mathbf{CI}_{\mathcal{B}}\text{-LS}_x$ dTM (similar derivation for other dTMs):

$$\frac{\partial p_1}{\partial A_{(q,r,s)}^l} = \frac{\partial \sigma(1 - h_0)}{\partial A_{(q,r,s)}^l} = \frac{\partial \sigma(1 - \vartheta_0(\mathcal{B}) - x^T \beta)}{\partial A_{(q,r,s)}^l} = \frac{\partial \sigma(\vartheta_0(\mathcal{B}))}{\partial A_{(q,r,s)}^l} = \sigma(\vartheta_0(\mathcal{B})) \cdot (1 - \sigma(\vartheta_0(\mathcal{B}))) \cdot \frac{\partial \vartheta_0(\mathcal{B})}{\partial A_{(q,r,s)}^l}.$$

We obtain an expression comprising only derivable components and the gradient of $\vartheta_0(\mathcal{B})$ corresponding to the output node which is determined automatically via backpropagation. An importance measure

for each activation map is obtained with global-average-pooling

$$\alpha_l^1 = \frac{1}{R \cdot S} \sum_q \sum_r \sum_s \frac{\partial p_1}{\partial A_{qrs}^l}.$$

Then, a weighted average across all activation maps is calculated and negative entries are removed such that

$$L_1^{\text{Grad-CAM}} = \text{ReLU} \left(\sum_l \alpha_l^1 \cdot A^l \right).$$

The final 3D explanation map is obtained by upsampling the map to the original input size. We obtain five 3D explanation maps per test patient due to the ensembling strategy that is used for optimizing the prediction performance. These maps are averaged using the weights of the joint transformation function from the ensemble dTM. Subsequently, the resulting 3D explanation map is overlaid with the original 3D brain image and then averaged along the axial direction to provide an interpretable 2D image with highlighted brain regions (s. Figure 3).

Occlusion: Occlusion is performed by systematically covering parts of the 3D input image and considering changes in the outcome prediction for the predicted class k before and after occlusion. Regions, in which the probability for the predicted class drops when being occluded, are considered being important. In case of our 3D images, we use a occlusion size of 18x18x4 and a stride width of 10x10x3, i.e. each voxel is occluded several times. To determine voxel importance we average the changes in predicted probability. To highlight only regions which support the predicted class, we set the importance value to zero when occluding a voxel results on average in a higher probability for the predicted class.

Due to deep ensembling, we again receive five 3D occlusion maps per test patient which are averaged using the weights from the ensembling. The resulting 3D explanation map is overlaid with the 3D brain image. Averaging in axial direction provides a interpretable 2D image as shown in Figure 3.

3 Results

Prediction performance: Although the focus of this study is not on prediction performance, a model with a reasonable prediction performance is necessary to receive meaningful explanation maps. Table 1 shows that all input modalities help to predict the outcome when we compare the performance to the null model **SI**. Models based on tabular data and a combination of tabular and imaging data achieve considerably higher prediction performances than dTMs using imaging data only.

	SI	CI_B	SI-LS_x	CI_B-LS_x
NLL	0.478 [0.423, 0.536]	0.452 [0.379, 0.528]	0.368 [0.308, 0.433]	0.384 [0.306, 0.47]
AUC	0.498 [0.430, 0.570]	0.714 [0.649, 0.777]	0.809 [0.747, 0.867]	0.812 [0.752, 0.868]
Specificity	1.0 [0.989, 1.0]	0.792 [0.745, 0.832]	0.783 [0.736, 0.824]	0.795 [0.749, 0.835]
Sensitivity	0.0 [0.0 , 0.049]	0.48 [0.371, 0.591]	0.627 [0.514, 0.727]	0.64 [0.527, 0.739]
Accuracy	0.816 [0.775, 0.850]	0.735 [0.69 , 0.775]	0.754 [0.71 , 0.794]	0.767 [0.723, 0.805]
F1-score	0.0 [0.0 , 0.0]	0.4 [0.307, 0.489]	0.485 [0.395, 0.568]	0.503 [0.413, 0.587]

Table 1: Test prediction performance for different dTMs: the SI model (Null model, where neither imaging nor tabular data are used), CI_B (based on imaging data), SI-LS_x (based on tabular data), and CI_B-LS_x model (based on imaging and tabular data). As performance measures NLL, AUC, specificity, sensitivity, accuracy, and the F1-Score are presented - lower NLL values indicate better performance, for all other measures higher values are better. NLL and AUC are most meaningful, because we are interested in correct probability predictions and face a quite imbalanced outcome. Bold numbers indicate best performance.

Explanation maps: Figure 4 shows the average across all explanation maps of patients predicted having a favorable or unfavorable outcome using the models CI_B or CI_B-LS_x when applying the adapted

Occlusion and Grad-CAM method. Both explanation methods show similar results. However, Grad-CAM explanation maps are smoother and the importance of specific image regions can be better identified due to a wider color spectrum. The visualized patterns can serve as basis for developing hypotheses about specific image features. For instance, we hypothesize that the highlighted frontal lobe in the CI_B model is important for predicting an unfavorable outcome due to its correlation with age. Increasing age is known to be associated with unfavorable functional outcome and with increasing age, the brain shrinks which is often most notable in the frontal and temporal cortex [13, 14]. This hypothesis is supported by the observation, that the frontal lobe is no longer highlighted when age is added to the model in terms of a tabular feature (s. CI_B-LS_X model).

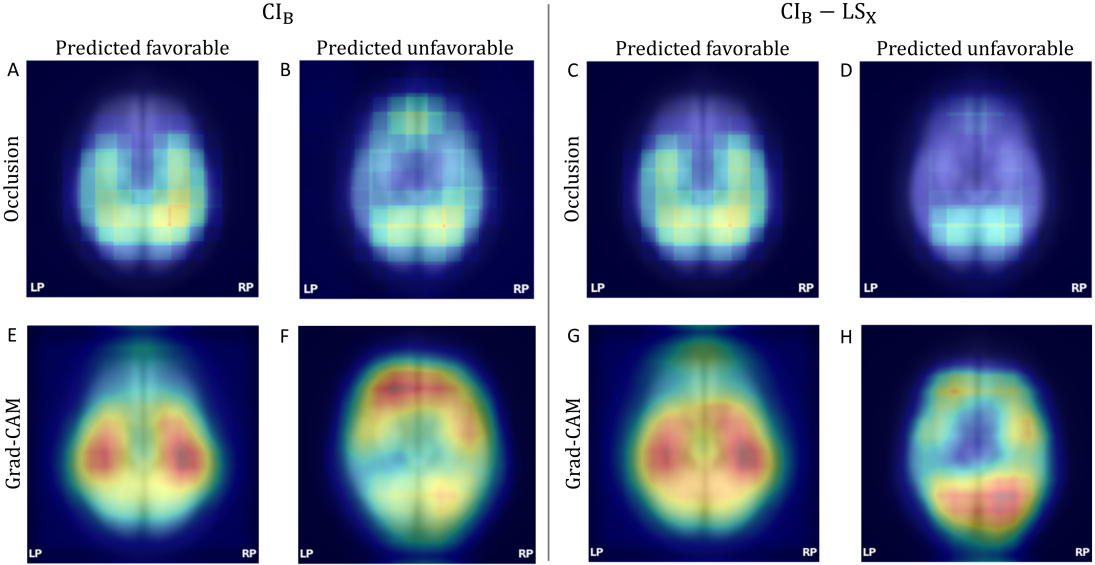


Figure 4: Average explanation maps. The figure shows the average across the explanation maps for patients predicted having a favorable or unfavorable outcome. The explanation maps correspond to the CI_B (left column) and CI_B-LS_X (right column) model when applying the Occlusion (upper row) or Grad-CAM (lower row) algorithm.

Figure 5 shows a similarity plot of individual Grad-CAM explanation maps resulting from the CI_B-LS_X model. The similarity plot is obtained with t-SNE using the feature-representations of the explanation maps which are extracted from the last convolutional layer of a ResNet-50 trained on Imagnet [15]. An interactive plot is available under https://liherz.shinyapps.io/tsne_xAI_shinyio/. The plot allows to identify groups of different characteristic image feature/brain regions important for outcome prediction and perform an error analysis. For example, when the model focuses on the whole brain and stroke location (lower left), patients are generally predicted correctly as having a favorable outcome. Dark explanation maps (upper right part) are mostly generated in TIA patients (with no visible lesion) or when the stroke appears as a big white blurred area. Those patients are (often falsely) predicted having an unfavorable outcome.

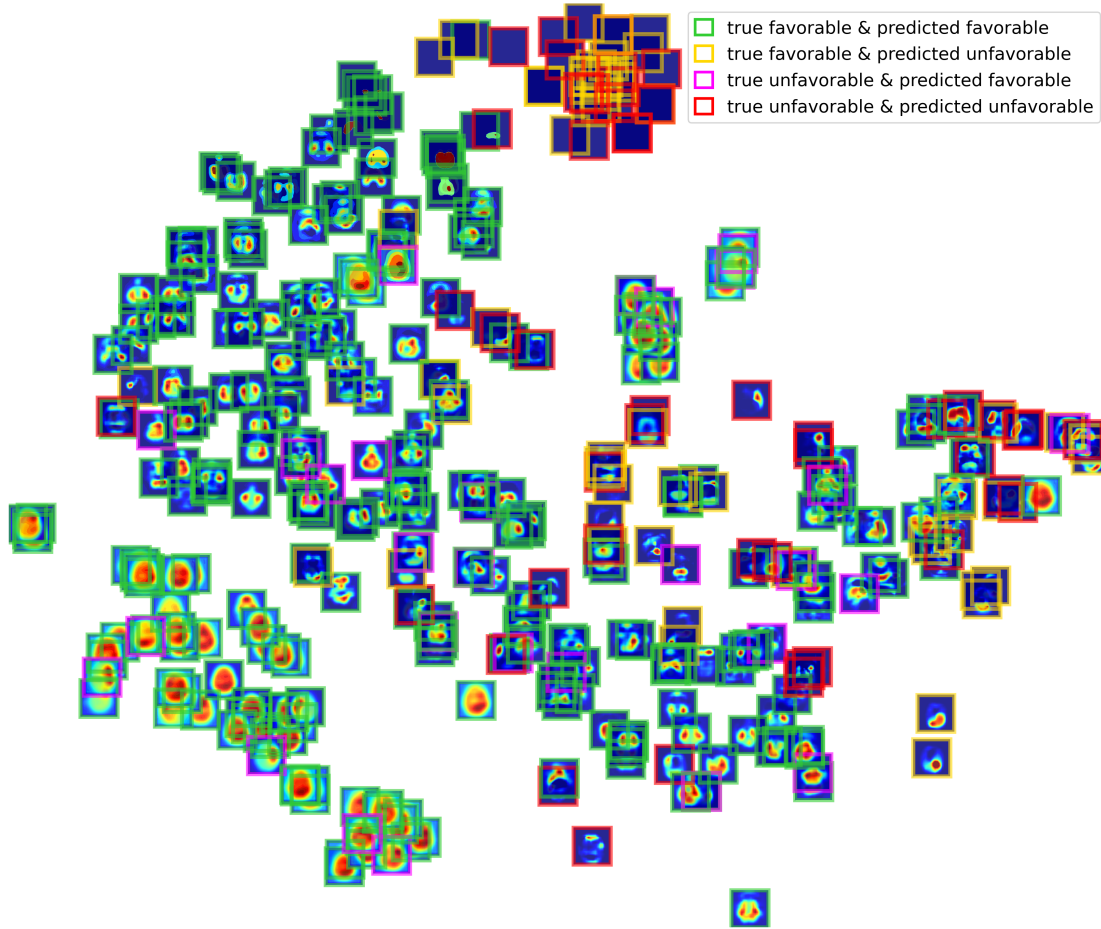


Figure 5: Similarity map. The figure shows a t-SNE plot for $\text{CI}_{\text{B}} - \text{LS}_{\text{X}}$ Grad-CAM explanation maps to indicate classes of brain regions for patients with correctly and wrongly predicted favorable and unfavorable outcome. The similarity map is obtained with t-SNE based on feature vectors extracted from a pretrained ResNet-50 architecture trained on Imagenet.

Interpretable model parameters: Besides explanation maps for imaging data, dTMs provide interpretable parameters for tabular features. Figure 6 summarizes the estimated parameters $\hat{\beta}$ of the linear shift terms $x^T \beta$ of the SI-LS_{X} and $\text{CI}_{\text{B}} - \text{LS}_{\text{X}}$ model which are directly interpretable as log-odds ratios like in standard logistic regression. Both, the SI-LS_{X} and $\text{CI}_{\text{B}} - \text{LS}_{\text{X}}$ model indicates that patients with higher pre-stroke mRS (being more dependent before the ischemic event) and increasing NIHSS on admission, i.e. more severe ischemic events, are more likely to have an unfavorable outcome at three months.

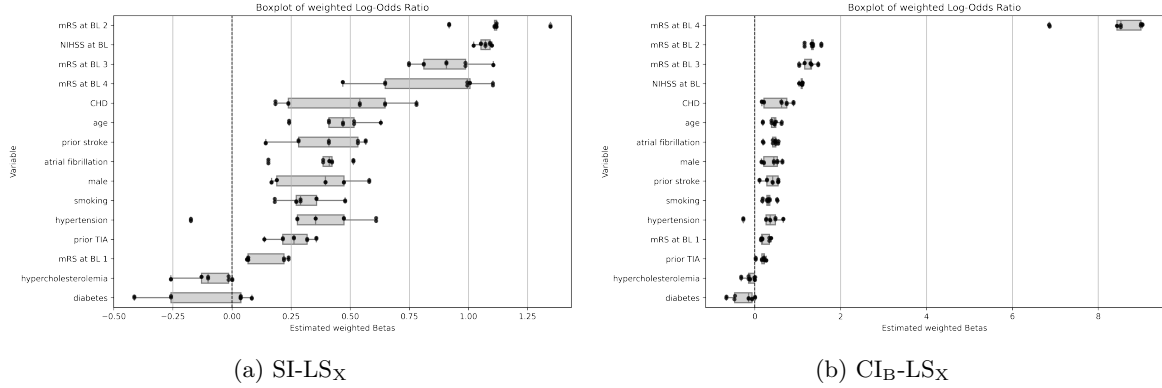


Figure 6: Estimated log-odds-ratios with 95% bootstrap CIs resulting from the linear shift part of the SI-LS_X model (left) and CI_B-LS_X model (right). Per predictor, we receive 10 estimates resulting from the 10 CV splits. In case of the CI_B-LS_X each parameter is averaged across the 5 ensemble members. Please note that not all 10 points are visible due to overlaid plotting. Categorical features (sex, smoking, hypertension, prior stroke or TIA, atrial fibrillation, coronary heart disease (CHD), diabetes, hypercholesterolemia, pre-stroke mRS (mRS at BL)) are shown with respect to the reference level. Coefficients for numeric variables (age, National Institutes of Health Stroke Scale on admission (NIHSS at BL)) are based on the standardized features.

4 Discussion

In this paper, we adapted the Occlusion and Grad-CAM methods to deep transformation models (dTMs) for multi-modal input data. We developed dTMs for predicting favorable vs. unfavorable outcome in patients with an ischemic event using 3D brain imaging and tabular data. We have shown that dTMs reliably predict functional outcomes with AUC values close to 0.8. In future applications, the incorporation of more data or the use of a pretrained foundation imaging model may further improve prediction performance of dTMs. For tabular features, dTMs yield fully interpretable parameters that quantify the effect of the features on the predicted outcome. The explanation maps resulting from the adapted Grad-CAM and Occlusion methods have highlighted similar image regions as being important for the same prediction. Grad-CAM provided smoother maps with a wider color spectrum and did not require additional prediction cycles, making it preferable over occlusion maps. Yet, both xAI methods provided consistent and meaningful insights into stroke pathophysiology and enable to identify potentially novel predictive image features. Moreover, some characteristic patterns in the explanation maps can indicate false predictions.

In summary, dTMs combine the best of deep learning (DL) models and statistical approaches to develop models that are reliable and applicable to life science fields, where transparent models are needed to handle multi-modal data and assess the trustworthiness of predictions. By adapting explanation maps to multi-modal dTMs, we have made the image model part explainable, providing the possibility for error analysis and the generation of hypothesis about novel image features relevant for outcome prediction.

References

- [1] C. Rudin, “Stop explaining black box machine learning models for high stakes decisions and use interpretable models instead,” *Nature Machine Intelligence*, vol. 1, p. 206–215, 2019.
- [2] L. L. Kook & Herzog, T. Hothorn, O. Dürr, and B. Sick, “Deep and interpretable regression models for ordinal outcomes,” *Pattern Recognition*, vol. 122, p. 108263, 2022.
- [3] P. F. Baumann, T. Hothorn, and D. Rügamer, “Deep conditional transformation models,” in *Joint European Conference on Machine Learning and Knowledge Discovery in Databases*, pp. 3–18, Springer, 2021.
- [4] L. Herzog, L. Kook, A. Götschi, K. Petermann, M. Hänsel, J. Hamann, O. Dürr, S. Wegener, and B. Sick, “Deep transformation models for functional outcome prediction after acute ischemic stroke,” *Biometrical Journal*, vol. 65, no. 6, p. 2100379, 2023.
- [5] L. Herzog, L. Kook, J. Hamann, C. Globas, M. R. Heldner, D. Seiffge, K. Antonenko, T. Dobrocky, L. Panos, J. Kaesmacher, *et al.*, “Deep learning versus neurologists: functional outcome prediction in lvo stroke patients undergoing mechanical thrombectomy,” *Stroke*, vol. 54, no. 7, pp. 1761–1769, 2023.
- [6] S. Bacchi, T. Zerner, L. Oakden-Rayner, T. Kleinig, S. Patel, and J. Jannes, “Deep learning in the prediction of ischaemic stroke thrombolysis functional outcomes: A pilot study,” *Academic Radiology*, vol. 27, pp. 19–23, 2020.
- [7] B. H. M. van der Velden, H. J. Kuijf, K. G. A. Gilhuijs, and M. A. Viergever, “Explainable artificial intelligence (xai) in deep learning-based medical image analysis,” *Medical Image Analysis*, vol. 79, July 2022.
- [8] M. D. Zeiler and R. Fergus, “Visualizing and understanding convolutional networks,” in *Computer Vision—ECCV 2014: 13th European Conference, Zurich, Switzerland, September 6–12, 2014, Proceedings, Part I 13*, pp. 818–833, Springer, 2014.
- [9] R. R. Selvaraju, M. Cogswell, A. Das, R. Vedantam, D. Parikh, and D. Batra, “Grad-cam: Visual explanations from deep networks via gradient-based localization,” in *Proceedings of the IEEE international conference on computer vision*, pp. 618–626, 2017.
- [10] K. Simonyan and A. Zisserman, “Very deep convolutional networks for large-scale image recognition,” *arXiv preprint arXiv:1409.1556*, 2014.
- [11] T. Hothorn, T. Kneib, and P. Bühlmann, “Conditional transformation models,” *Journal of the Royal Statistical Society. Series B: Statistical Methodology*, vol. 76, no. 1, pp. 3–27, 2014.
- [12] L. Kook, A. Götschi, P. Baumann, T. Hothorn, and B. Sick, “Deep interpretable ensembles,” *arXiv*, 05 2022.
- [13] A. M. Fjell and K. B. Walhovd, “Structural brain changes in aging: courses, causes and cognitive consequences,” *Reviews in the Neurosciences*, vol. 21, pp. 187–221, 2010.
- [14] P. R., “Ageing and the brain,” *Postgraduate Medical Journal*, vol. 82, pp. 84–88, Feb. 2006.
- [15] K. He, X. Zhang, S. Ren, and J. Sun, “Delving deep into rectifiers: Surpassing human-level performance on imagenet classification,” *IEEE International Conference on Computer Vision*, 2015.